HHS Public Access

Author manuscript

Acta Biomater. Author manuscript; available in PMC 2019 January 15.

Published in final edited form as:

Acta Biomater. 2018 September 15; 78: 365–377. doi:10.1016/j.actbio.2018.07.039.

Functionally graded multilayer scaffolds for *in vivo* osteochondral tissue engineering

Heemin Kang[d], **Yuze Zeng**[b,c], and **Shyni Varghese**[a,b,c,d,e,*]

[a]Department of Biomedical Engineering, Duke University, Durham, NC 27710, United States

[b]Department of Mechanical Engineering and Materials Science, Duke University, Durham, NC 27710, United States

[c]Department of Orthopaedic Surgery, Duke University, Durham, NC 27710, United States

[d]Materials Science and Engineering Program, University of California, San Diego, La Jolla, CA 92093, United States

[e]Department of Bioengineering, University of California, San Diego, La Jolla, CA 92093, United States

Abstract

Osteochondral tissue repair remains a significant challenge in orthopedic surgery. Tissue engineering of osteochondral tissue has transpired as a potential therapeutic solution as it can effectively regenerate bone, cartilage, and the bone-cartilage interface. While advancements in scaffold fabrication and stem cell engineering have made significant progress towards the engineering of composite tissues, such as osteochondral tissue, new approaches are required to improve the outcome of such strategies. Herein, we discuss the use of a single-unit trilayer scaffold with depth-varying pore architecture and mineral environment to engineer osteochondral tissues *in vivo*. The trilayer scaffold includes a biomineralized bottom layer mimicking the calcium phosphate (CaP)-rich bone microenvironment, a cryogel middle layer with anisotropic pore architecture, and a hydrogel top layer. The mineralized bottom layer was designed to support bone formation, while the macroporous middle layer and hydrogel top layer were designed to support cartilage tissue formation. The bottom layer was kept acellular and the top two layers were loaded with cells prior to implantation. When implanted *in vivo*, these trilayer scaffolds resulted in the formation of osteochondral tissue with a lubricin-rich cartilage surface. The osteochondral tissue formation was a result of continuous differentiation of the transplanted cells to form cartilage tissue and recruitment of endogenous cells through the mineralized bottom layer to form bone tissue. Our results suggest that integrating exogenous cell-based cartilage tissue engineering along with scaffolddriven *in situ* bone tissue engineering could be a powerful approach to engineer analogs of osteochondral tissue. In addition to offering new therapeutic opportunities, such

*Corresponding author at: Department of Biomedical Engineering, Duke University, Durham, NC 27710, United States, shyni.varghese@duke.edu (S. Varghese).

Author contributions

H.K., Y.Z., and S.V. designed research; H.K. and Y.Z. performed research; H.K., Y.Z., and S.V. analyzed data; and H.K., Y.Z., and S.V. wrote the manuscript.

The authors declare no conflict of interest.

approaches and systems could also advance our fundamental understanding of osteochondral tissue regeneration and repair.

Keywords

Biomimetic materials; Trilayer scaffold; Pore architecture; Biomineralization; Osteochondral tissue

1. Introduction

Cartilage lesions are common and often irreparable due to the inherently compromised regeneration capacity of native cartilage tissues [1]. As the cartilage lesions progress, they often extend to underlying subchondral bone, making the repair of both cartilage and underlying bone tissue a requirement. Implantation of osteochondral tissues has been thought to be an effective strategy for treating cartilage defects [2]. In addition to promoting integration of the implanted tissue with the subchondral bone, the engineered osteochondral tissue can also facilitate the communication between the subchondral bone and the cartilage layer, which plays an important role in cartilage tissue formation [3].

To create osteochondral tissues, tissue engineering strategies that leverage biomaterials and cells have been extensively studied [4–10]. Many of these approaches mimic the heterogeneous and layered architecture of native osteochondral tissue. One such approach includes physical integration of engineered cartilage tissue with the decellularized bone tissue [11]. An alternative approach is the use of multi-layered scaffolds designed to provide pro-osteogenic and pro-chondrogenic environment in a layered fashion to support cartilage and bone tissues simultaneously [12]. Such multilayer scaffolds loaded with stem cells or stem cell-derived chondrocytes and osteoblasts have been studied extensively to engineer osteochondral tissues both *in vitro* and *in vivo* [13,14]. The premise of these studies mostly relies on our understanding that the biomaterial-based cues can be used to direct various cellular functions including the differentiation of stem cells into chondrocytes and osteoblasts.

Bone marrow derived stromal stem cells (MSCs) are a promising cell source for osteochondral tissue engineering [15]. In addition to their ability to undergo osteogenic and chondrogenic differentiation, multipotent MSCs can be collected from patients and thus making it patient-specific [16]. Cocktail medium containing both osteogenicand chondrogenic-inducing components, and/or scaffolds decorated with tissue-specific physicochemical cues including spatially confined growth factors have been used to guide differentiation of the encapsulated cells towards chondrocytes and osteoblasts lineages [17–23]. However, it is still challenging to generate discrete cartilage and bone tissues concurrently from MSCs within a single scaffold. Grayson et al. have investigated the effect of preconditioning and/or the use of cocktail medium containing chondrogenic and osteogenic-inducing components on the formation of osteochondral tissue [24]. Their results showed that while pre-conditioning and cocktail medium promoted bone tissue formation, there was a negative effect on cartilage tissue formation. These studies illustrate the opportunities and challenges associated with tissue engineering of composite tissues

containing different cell populations and the importance of new approaches to advance the outcome.

In this study, we determine the ability of an integrated approach which utilizes endogenous cell-mediated *in situ* bone tissue engineering along with exogenous cell-mediated cartilage tissue engineering to form discrete bone and cartilage tissues in a layered fashion within a single scaffold. This was achieved with the help of a trilayer scaffold with spatially varying pore architecture and mineral environment. The acellular bottom layer of the trilayer scaffold was mineralized so as to form bone tissue by recruiting endogenous cells upon *in vivo* implantation, while the cellular middle layer with columnar macroporous structure and the hydrogel top layer encapsulated with human mesenchymal stem cell (hMSC) aggregates were designed to support viability and function of exogenous cells and cartilage tissue formation. Our results show that this approach can successfully yield osteochondral tissue *in vivo*.

2. Materials and methods

2.1. Synthesis of the bottom and middle layers

Synthesis of poly(ethylene glycol)-diacrylate (PEGDA, Mn = 3.4 kDa) and N-acryloyl 6-aminocaproic acid (A6ACA) was carried out as previously described [23,25]. The macroporous bottom and middle layers of the trilayer scaffold were manufactured as a single bilayer system with depth-varying pore architecture through cryogelation [26]. Briefly, the macroporous bottom layer with interconnected pore structures was synthesized by dispensing 30 μL of chilled precursor solution containing 20% (w/v) PEGDA and 0.5 M A6ACA in 0.5 N NaOH with 0.5% (w/v) ammonium persulfate (APS) and 0.2% (v/v) N,N,N′-N′-tetramethylethylenediamine (TEMED) into a frozen cylindrical polypropylene mold (5 mm in diameter) and allowing it to polymerize at 20 °C for 24 h. The macroporous middle layer with columnar pore structures was prepared by adding 40 μL of chilled precursor solution containing 20% (w/v) PEGDA in deionized (DI) water with 0.5% (w/v) APS and 0.2% (v/v) TEMED onto the surface of the previously formed frozen bottom layer and allowing it to polymerize at 20 °C for 24 h. The frozen bilayer product was then placed into phosphate-buffered saline (PBS), which yielded a single macroporous cryogel with distinct depth-varying pore architecture. The schematic in Fig. 1A shows the step-wise fabrication procedure. The resulting bilayer structure was washed in PBS three times, exhibiting 8 mm in diameter with approximately 2 mm and 2.5 mm in thickness for the bottom and the middle layer, respectively.

2.2. Biomineralization of the bottom layer

The PEGDA-*co*-A6ACA bottom layer of the bilayer cryogel was biomineralized as reported elsewhere [27]. Briefly, the bilayer cryogel was equilibrated in DI water for 6 h and soaked in modified simulated body fluid (m-SBF, pH = 7.4) at 25 °C for 6 h. The m-SBF solution consists of 142.0 mM Na^+, 5.0 mM K^+, 1.5 mM Mg^{2+}, 2.5 mM Ca^{2+}, 103.0 mM Cl^-, 10.0 mM HCO_3^-, 1.0 mM HPO_4^{2-}, and 0.5 mM SO_4^{2-}. The resulting cryogel was briefly rinsed with DI water and incubated in 40 mM Ca^{2+} and 24 mM HPO_4^{2-} solution (pH = 5.2) at 25 °C

for 30 min on a rotating shaker (VWR, Cat. # 12620938) at 200 rpm. It was then briefly rinsed with DI water, incubated in m-SBF at 37 °C for 2 d with daily change of m-SBF, and washed with PBS to obtain a biomineralized bottom layer.

The bilayer cryogel was then sterilized by soaking in 70% ethanol for 6 h. The ethanol-treated cryogel was washed with sterile PBS for 5 days with four times of daily change of PBS to ensure complete removal of the residual ethanol. The sterilized bilayer cryogel was saved for cell loading and addition of a top layer.

2.3. Cell culture

Human mesenchymal stem cells (hMSCs) were obtained from Institute for Regenerative Medicine at Texas A&M University. hMSCs were maintained in growth medium containing high glucose DMEM, 10% (v/v) fetal bovine serum (FBS, HyClone), 4 mM L-glutamine, and 50 U/mL penicillin/streptomycin. hMSCs were passaged atapproximately 70–80% confluency. Passage 5 (P5) hMSCs were used for the experiments. To generate hMSC aggregates of ~ 100 μm in diameter, a rotational method was adopted as described elsewhere [28]. Briefly, approximately 1 million hMSCs were suspended in 10 mL of growth medium in a petri dish (10 cm in diameter) under gentle rotation at 100 rpm for 1 d by using an orbital shaker. hMSCs were loaded into the middle layer while the hMSC aggregates were used for the hydrogel top layer.

Chondrocytes were isolated as reported earlier [29]. Briefly, articular cartilage was dissected from femoral condyle and patellar groove of 8-week-old bovine legs. The dissected cartilage pieces were digested in DMEM containing 0.15% (w/v) collagenase (Worthington Biochemical, Cat. # LS004177) and 5% (v/v) FBS for 16 h at 37 °C and 5% CO_2 to isolate chondrocytes. The cell suspension was filtered through 70 μm nylon cell strainer (Falcon) and washed with PBS containing 50 U/mL penicillin/streptomycin. The isolated primary chondrocytes along with hMSCs were loaded into the middle layer of the trilayer scaffold.

2.4. Cell-laden scaffold

To generate a cell-laden trilayer scaffold, the sterilized bilayer cryogel was incubated in growth medium at 37 °C for 1 d prior to cell loading. About 35 μL of the fluid was removed from the incubated cryogel by using a pipette, yielding ~50% weight loss. Then, 35 μL of cell suspension including 1.05 million P5 hMSCs and 0.45 million primary chondrocytes (hMSCs: chondrocytes = 70:30) was loaded into the middle layer. The cell-laden bilayer cryogel was incubated at 37 °C and 5% CO_2 for 2 h to allow cell infiltration before being transferred into 1.5 mL of growth medium. After 1 d, hMSC aggregates-laden hydrogel layer was formed onto this bilayer scaffold. Briefly, hMSC aggregates (~100 μm in diameter generated from 1 million of P5 hMSCs) were suspended in 15 μL of a precursor solution containing 10% (w/v) PEGDA and 0.05% (w/v) Irgacure 2959 (Sigma-Aldrich, Cat. # 410896). The cell aggregates-dispersed precursor solution was dispensed onto the bilayer scaffold and subjected to photopolymerization under UV light for 5 min. This top hydrogel layer of the trilayer scaffold exhibited 0.5 mm in thickness. The encapsulated hMSC aggregates were visualized by bright-field images and the approximate size of the aggregates

was determined by measuring 30 aggregates from multiple images with ImageJ. The data were presented as mean ± standard errors.

The cell-laden trilayer scaffold with an acellular mineralized bottom layer was cultured in chondrogenic-inducing medium at 37 °C and 5% CO_2 with medium change every two days. Some of these scaffolds were used for subcutaneous implantation after 1 week of pre-conditioning while others were kept *in vitro*. The tissue-engineered scaffolds were characterized at 4 and 8 weeks of post-implantation. Chondrogenic-inducing medium was prepared by supplementing DMEM with 1% (v/v) Corning ITS Premix Universal Culture Supplement (CB-40352), 100 nM dexamethasone (Sigma-Aldrich, Cat. # D2915), 40 μg/mL L-Proline (SigmaAldrich, Cat. # P5607), 50 μg/mL L-Ascorbic acid 2-phosphate (Sigma-Aldrich, Cat. # A8960), 100 μg/mL sodium pyruvate (Life Technologies, Cat. # 11360–070), 50 U/mL penicillin/streptomycin, and 10 ng/mL human recombinant TGF-β1 (Fitzgerald, Cat. # 30RAT027).

2.5. Scanning electron microscopy (SEM) and energy-dispersive spectroscopy (EDS)

SEM imaging was used to characterize the pore architecture and confinement of minerals within the bottom layer. To examine the elements of the minerals and determine their composition, EDS analysis was carried out. The trilayer scaffold was briefly rinsed with DI water, cut into vertical sections of thin slices, which were subjected to flash-freezing followed by lyophilization. The samples were Iridium-coated for 7 s in the sputter (Emitech, Cat. # K575X) and were imaged by using SEM (Philips XL30 ESEM) for top, middle, and bottom layers of the trilayer scaffold as well as analyzed for elemental spectra by using integrated EDS system. INCA software was used to quantify the calcium to phosphate (Ca/P) atomic ratio of the minerals from the elemental spectra. The pore size in major and minor axes for middle and bottom layer of the trilayer scaffold was calculated from 30 pores chosen from multiple SEM images by using ImageJ. Pore aspect ratio was determined as a ratio of pore size in major axis to minor axis for both middle and bottom layer (n = 30).

2.6. Live-dead staining

To examine the viability and distribution of loaded cells and encapsulated aggregates, live-dead staining was conducted. After 3 d in chondrogenic-inducing medium, the scaffolds were sliced into vertical sections and washed with PBS. The flat slices were incubated in DMEM containing 0.05% (v/v) green-fluorescent calcein-AM and 0.2% (v/v) red-fluorescent ethidium homodimer1 at 37 °C for 30 min using Live/Dead Cell Viability Assays kit (Life technologies, Cat. # L-3224). The stained sections were washed with PBS and imaged for top, middle, and bottom layer of the scaffolds using a fluorescence microscope (Carl Zeiss, Axio Observer. A1).

2.7. Subcutaneous implantation

All animal studies were carried out with the approval of the Institutional Animal Care and Use Committee (IACUC) at University of California, San Diego and in accordance with NIH guidelines for laboratory animal care. All *in vivo* experiments were repeated independently at least once. Pre-conditioned scaffolds (cultured *in vitro* in chondrogenic-inducing medium for 1 week) of 8 mm in diameter and 5 mm in height were implanted

subcutaneously into immunodeficient mice (NOD.CB17-Prkdcscid/J, 3-month-old). The mice were administered with ketamine (Ketaset, 100 mg/kg) and xylazine (AnaSed, 10 mg/kg) through an intraperitoneal injection. The anesthetized mice were subjected to a 1.5 mm-long incision on their back and four subcutaneous pouches (cranial-left, cranial-right, caudal-left, and caudal-right) were exposed for implantation. After implantation, the skin was closed with sutures. A total of 32 cell-laden trilayer scaffolds were implanted. The scaffolds were excised as a function of postimplantation time (0, 4, and 8-weeks) and analyzed. Osteochondral tissues from the hind limbs were used as positive controls.

2.8. Micro-computed tomography (μCT)

To evaluate *in vitro* and *in vivo* calcification within the cellladen trilayer scaffolds, μCT analysis was carried out. The scaffolds were collected after 1, 5, and 9 weeks of *in vitro* culture and the implants were retrieved from mice at 0, 4, and 8 weeks postimplantation. All samples were fixed in 4% paraformaldehyde at 4 °C for 4 d. The fixed samples were tightly placed between Styrofoam disks in 15 mL centrifuge tubes. The scaffolds were scanned using SkyScan 1076 μCT scanner (Bruker, pixel resolution: 9 μm, 50 kV, Al filter). The scanned images were reconstructed by using NRecon software (SkyScan, Bruker) and assembled into 3D models by using CT Analyzer software (SkyScan, Bruker) with a threshold range of 70–255. 360° rotation of 3D images was constructed by using CTvol software (SkyScan, Bruker, 24 frames with each frame at 15° rotation). Calcification density of the scaffolds was determined from the 3D images with a threshold range of 70–255 by selecting six different areas in each layer (top, middle, and bottom). The reconstructed images of the scaffolds were converted into 2D coronal cross-sectional images to demonstrate a planar view of the calcified tissue by using DataViewer software (SkyScan, Bruker).

2.9. Preparation for histological staining

Sections of scaffolds embedded in paraffin were used for histological analyses. The tissue-engineered scaffolds (both *in vitro* and *in vivo*) as well as native osteochondral tissues were fixed with 4% paraformaldehyde at 4 °C for 4 d, demineralized in 10% ethylenedi aminetetraacetic acid (EDTA, pH = 7.3) at 4 °C for 7 d, and washed with PBS for 6 h. The demineralized samples were dehydrated, equilibrated in CitriSolv solution for 1 h, and incubated in a molten mixture of 95 w/w% paraffin and 5 w/w% poly(ethylene-*co*-vinyl acetate) (Sigma Aldrich, Cat. # 437220) at 70 °C under vacuum for 1 d. The paraffin-embedded samples were sliced into 10 μm-thick vertical sections using a microtome (Leica, RM2255). Prior to staining, the sections were de-paraffinized in CitriSolv for 15 min and rehydrated.

2.10. Hoechst staining

The rehydrated sections were incubated with Hoechst 33342 solution (2 μg/ml, Life Technologies, Cat. # H21492) at 25 °C for 10 min and washed with PBS. The stained sections were imaged using a fluorescence microscope.

2.11. Histochemical staining

For hematoxylin and eosin (H&E) staining, the rehydrated sections were incubated in hematoxylin solution (Ricca, Cat. # 3536–16) for 4 min and washed with DI water. The sections were then immersed in Eosin-Y solution (Richard-Allan Scientific, Cat. # 7111) for 1 min and washed with DI water. For Alcian Blue staining, the rehydrated sections were stained in a solution containing 1% (w/v) Alcian Blue (National Diagnostics, Cat. # HS-504) in 0.1 M HCl (pH = 1.0) for 1 h. The stained sections were washed with 0.1 M HCl. The stained sections (H&E and Alcian Blue) were imaged using a microscope in a color mode.

2.12. Immunohistochemical staining

For immunohistochemical staining against type I, II, and X collagen, osteocalcin, lubricin, and lamin B, the rehydrated sections were incubated with 20 μg/mL proteinase K solution (Invitrogen, Cat. # 100005393) in a mixed solution of 95% (v/v) TE buffer (50 mM Tris-HCl and 1 mM EDTA, Triton X-100, pH = 8.0) and 5% (v/v) glycerol for 15 min at 37 °C and washed with PBS. The treated sections were immersed in a blocking solution containing 3% (w/v) normal goat serum and 0.1% (v/v) Triton X-100 at 25 °C for 1 h and incubated with primary antibodies against type I collagen (1:100, rabbit polyclonal, Fitzerald, 70R-CR007x), type II collagen (1:50, rabbit polyclonal, Fitzerald, 70R-CR008), type X collagen (1:50, rabbit polyclonal, Fitzerald, 20R-CR030), osteocalcin (1:100, rabbit polyclonal, Abcam, ab93876), lubricin (1:50, goat polyclonal, Santa Cruz Biotechnology, sc-50079), or lamin B (1:100, rabbit polyclonal, Thermo Scientific, RB10569-P0) in a blocking solution at 4 °C for 16 h. The sections were washed with PBS and treated with 3% (v/v) hydrogen peroxide for 7 min to deactivate endogenous peroxidase. The treated sections were incubated with horseradish peroxidase (HRP)-conjugated secondary antibodies against rabbit (1:200, donkey anti-rabbit, Jackson ImmunoResearch, 711-035-152) or goat (1:100, donkey anti-goat, Jackson ImmunoResearch, 705–035-003) in a blocking solution at 25 °C for 1 h and washed with PBS. The sections were immersed in a developing solution containing 3–30 diaminobenzidine (DAB) substrate (Vector Laboratories, SK-4100) for 5 min in presence of peroxidase and washed with PBS. The immunohistochemically stained sections were imaged using a microscope in a color mode.

2.13. Biochemical assays

The scaffolds were collected 8 weeks post subcutaneous implantation. Half of them were used intact (the trilayer, n = 8), while the other half were used after separating the cartilage layer (the middle and top layers, n = 8) from the bone layer (the bottom layer, n = 8). The wet and dry weights of the scaffolds were measured before and after lyophilization, respectively. Each dried sample was homogenized and digested in 1 mL of papain solution for 16 h at 60 °C. The papain solution was made by dissolving 125 mg/mL papain (Sigma, Cat. # P3125), 10 mM L-cysteine, and 10 mM EDTA in 100 mM phosphate buffer (pH 6.5).

The DNA content of the papain-digested samples was quantified by using PicoGreen dsDNA assay kit (Invitrogen) as per the manufacturer's instruction. Briefly, each papain-digested sample was diluted 200 folds in 1X TE working solution (10 mM Tris-HCl, 1 mM EDTA, pH 7.5) and mixed with an equal volume of 1X PicoGreen dsDNA reagent. The mixture was kept in dark at room temperature for 5 min. Fluorescence intensity was

measured using a Beckman Coulter DTX 880 Multimode Detector (excitation: 480 nm; emission: 520 nm). DNA concentration was extrapolated against a lambda DNA standard curve generated using a concentration range of 0 ng/mL to 1 μg/mL.

The sulfated glycosaminoglycan (sGAG) content was measured by using 1,9-dimethylmethylene blue (DMMB; Sigma-Aldrich, Cat. # 341088) spectrophotometric assay according to a published method [30]. Briefly, DMMB was dissolved in a solution containing 40 mM glycine, 40 mM NaCl and 10 mM HCl to yield a final concentration of 40 μM. Each papain-digested sample was diluted 100 folds in the DMMB solution and the absorbance of the resulting mixture was measured at 525 nm using a Beckman Coulter DTX 880 Multimode Detector. GAG concentration was extrapolated against a chondroitin sulfate standard curve with concentrations ranging from 0 μg/mL to 100 μg/mL.

The collagen content was determined by measuring hydroxyproline amounts in the samples as described earlier [30]. Briefly, each papain-digested sample was first diluted 10 folds in 6 M HCl and hydrolyzed at 120 °C for 18 h. The hydrolyzed samples were neutralized with 2.5 M NaOH and mixed with one drop of methyl red (a pH indicator). 1 mL of each resulting solution was mixed with 0.5 mL of 50 mM freshly prepared chloramine-T (Sigma-Aldrich, Cat. # 402869) and kept at room temperature for 30 min, followed by adding 0.5 mL of 1 M pDAB (Sigma-Aldrich, Cat. # 156477). After incubation for 30 min at 60 °C, the absorbance was measured at 550 nm. The collagen concentration was computed by using a hydroxyproline standard curve with concentrations ranging from 0 to 10 μg/mL, assuming a 7.5:1 collagen-tohydroxyproline mass ratio [31].

2.14. Statistical analysis

A sample size of $n \geq 6$ was used for all experiments. Each experiment was independently repeated at least twice. GraphPad Prism 5 was used to perform statistical analyses. Statistical significances were indicated as asterisks for *p*-values less than 0.05. Two-tailed Student's *t*-test was used to compare two groups at the same time point. One-way analysis of variance (ANOVA) with post-hoc TukeyKramer test was employed to compare multiple groups at the same time point.

3. Results

3.1. Trilayer scaffolds with anisotropic pore architecture and selective mineralization

Single-unit trilayer scaffolds with spatially varying pore architecture were developed from poly(ethylene glycol)-diacrylate-co6-aminocaproic acid copolymers as shown in Fig. 1. Specifically, the trilayer scaffold consisted of an interconnected macroporous bottom layer, a middle layer of macroporous columnar structure, and a hydrogel top layer. The bottom and middle layers were fabricated as a single macroporous cryogel with varying pore structures (interconnected and columnar pore architectures) in a layered fashion as previously described by us [26]. The hydrogel top layer was formed onto the macroporous bilayer cryogel, thus yielding an integrated trilayer scaffold with depth varying pore architecture. The SEM images of the scaffold showed the formation of a continuous structure with varying pore architectures (Fig. 1B, left). The pore sizes in the bottom layer along the major

and minor axes were 33.6 ± 13.2 μm and 27.4 ± 11.1 μm, respectively; and those in the middle layer were 132.6 ± 24.2 μm and 37.5 ± 8.6 μm, respectively (Fig. 1D). The corresponding pore aspect ratios for the bottom layer (1.3 ± 0.2) and the middle (3.6 ± 0.6) are shown in Fig. 1E. The bottom layer of the trilayer scaffold containing the carboxylic acid functional groups was selectively mineralized to incorporate calcium phosphate (CaP) minerals [27,32–34]. SEM images (Fig. 1B) and EDS analysis (Fig. 1C) revealed the presence of CaP minerals within the bottom layer, while no CaP minerals were present in the middle and top layers. The CaP minerals within the bottom layer have a Ca/P atomic ratio of 1.23.

3.2. Chondrogenic differentiation of hMSCs and cartilage tissue formation in vitro

To determine the ability of the middle and top layers of the trilayer scaffold (the layers that are designed for cartilage tissue engineering) to support cartilage tissue formation, bone marrow derived hMSCs were incorporated into the respective layers and cultured in chondrogenic-inducing medium (Fig. 2A). In the middle layer, hMSCs were co-cultured with primary bovine chondrocytes. The cells were loaded at a ratio of 70:30 (MSCs:Chondrocytes). The chondrocytes were included to promote chondrogenic differentiation of hMSCs and to prevent the hMSC-derived chondrogenic cells from undergoing hypertrophy [21,28,30,31,35]. hMSC aggregates of 98.9 ± 3.4 μm (Fig. S1) were encapsulated within the top layer where the aggregates were used to mimic the developmental mesenchymal condensation [11,36]. The mineralized bottom layer designed for bone tissue formation was kept acellular. Live-dead analyses after 3 days of *in vitro* culture showed that the loaded cells were viable and confined within the middle and top layers (Fig. 2B). Hoechst staining indicated no migration of cells to the mineralized bottom layer from the adjacent cell-laden layers even after 9 weeks of culture (Fig. 2C).

The cellladen scaffolds were cultured in chondrogenicinducing medium and characterized as a function of culture time (1, 5, and 9 weeks). H&E staining after 5 and 9 weeks of *in vitro* culture demonstrated chondrogenic differentiation of hMSCs and formation of cartilaginous-like tissue in the cell-laden top and middle layers (Fig. S2). Alcian blue staining as well as type II collagen staining showed the deposition of GAG and type II collagen respectively within the top and middle layers. In contrast, negligible levels of Alcian blue and collagen type II staining were detected in the bottom layer (Figs. S3 and S4). Negative staining for type X collagen in the top and middle layers of the scaffold suggests the absence of hypertrophic differentiation of hMSC-derived chondrocytes in the engineered cartilage tissue (Fig. S5). Minimal to negative staining for type I collagen and osteocalcin reveals no osteogenic differentiation of cells in the top and middle layers (Figs. S6 and S7). This is in agreement with the micro-computed tomography (μCT) images, which showed no significant calcification of the scaffolds during the course of the *in vitro* culture (Fig. S8).

3.3. Trilayer scaffold supports osteochondral tissue formation in vivo

In vitro studies validated the ability of the top and middle layers of the scaffold to support chondrogenic differentiation of the loaded cells in presence of chondrogenic medium. We next implanted the pre-conditioned scaffolds (*i.e.*, the trilayer scaffold with the top and middle layers populated with cells cultured *in vitro* in chondrogenic-inducing medium for 1

week) and examined their ability to support osteochondral tissue formation *in vivo* (Fig. 2A). To this end, the pre-conditioned scaffolds were implanted subcutaneously and characterized as a function of time (4 and 8 weeks post-implantation). Fig. 3A shows the gross appearance of the retrieved implants after 4 and 8 weeks. Fluorescent staining of the excised implants after 4 and 8 weeks implantation with Hoechst showed the presence of cells throughout the three layers (Fig. 3B), indicating the recruitment of host cells to the mineralized bottom layer. A random distribution of cells was observed within the top and bottom layers, whereas cells in the middle layer were vertically aligned as dictated by the columnar pore architecture of the layer (Fig. 3B). Cells in the top layer resided in lacunaelike structures and aligned near horizontally, recapitulating some aspects of the superficial zone of native cartilage. Quantitative PicoGreen analysis of the implants, which measures the amount of DNA, also suggests the presence of cells throughout the scaffold (Fig. 6A). Furthermore, human-specific lamin B staining of the scaffolds after 8 weeks of implantation showed positive signal only in the top and middle layers (Fig. S9), which further confirms that the cells in the bottom layers were recruited from the host and that the exogenous cells were confined within the top and middle layers.

Three-dimensional μCT images showed an increase in optical signal in the mineralized bottom layer over time, indicating further calcification of the mineralized layer of the implant *in vivo* (Fig. 4A and B). No such calcification was observed in the middle and top layers. 360° rotation views of the 3D μCT images and 2D coronal cross-sectional images of the implants at 4 and 8 weeks post-implantation further corroborate the observation that the calcification was confined within the bottom layer. The intensity of calcification in the bottom layer increased with implantation time (Movies S1 and S2; Fig. S10).

H&E staining of the implants showed formation of disparate cartilage and bone tissues in a layered fashion over 8 weeks postimplantation (Figs. 3C and S11). The bone tissue formed within the biomineralized bottom layer was positive for type I collagen staining after 4 and 8 weeks of implantation, while minimal type I collagen was detected within the top and middle layers (Figs. 4C and S12). Prevalent staining for osteocalcin, a bonespecific ECM protein secreted by osteoblasts, was found in the type I collagen-rich bottom layer at 4 and 8 weeks post-implantation, further confirming the presence of bone tissue within the mineralized bottom layer (Figs. 4C and S12). The tissue within the biomineralized layer also showed positive staining for type X collagen (Figs. 4C and S13). In stark contrast, tissues within the top and middle layers showed minimal to negative staining for type X collagen and osteocalcin.

Alcian Blue staining of the implants at 4 and 8 weeks postimplantation demonstrated significant amounts of GAG deposition throughout the top and middle layers as compared to the bottom layer (Figs. 5 and S14). Biochemical analyses of the implants further confirmed that majority of GAG was confined within the cartilage layer (Fig. 6C, D). Predominant staining for type II collagen, a cartilage-specific ECM protein, was found in the GAG-rich top and middle layers at 4 and 8 weeks post-implantation (Figs. 5 and S14). On the other hand, minimal staining for type II collagen was spotted in the bottom layer. Biochemical analyses of total collagen content confirmed the presence of collagen within the engineered tissue (Fig. 6E and F). Total collagen content was found to be higher in the bone layer than

in the cartilage layer when normalized to DNA content (Fig. 6E), indicating higher total collagen biosynthesis by cells in the bone layer. The seemingly opposite trend of total collagen content shown in Fig. 6F when normalized to dry weight is probably due to the weight contribution of minerals in the bone layer.

The top layer of the engineered tissue was stained positive for lubricin, which was exclusively found at the surface of the top layer at 4 and 8 weeks post-implantation (Figs. 5 and S14). Interestingly, the presence of lubricin was observed only in the *in vivo* engineered tissues (Fig. S15).

4. Discussion

In this study, we utilize *in vitro* cartilage tissue engineering using stem cells and mineralized scaffold-mediated *in situ* bone tissue engineering through the recruitment of endogenous cells to create osteochondral tissues *in vivo*. Integration of cryogelation with hydrogelation led to the development of a single-unit structure with depth-varying pore architecture. This results in a continuous multilayer structure with no physical barriers for composite tissue formation. Templated biomineralization via the A6ACA pendant chains present in the bottom layer was found to be effective in limiting the mineral environment to the bottom layer. The carboxyl groups of A6ACA moieties bind Ca^{2+} ions and promote nucleation and growth of calcium phosphate (CaP) minerals. In addition to the carboxyl groups, the length of the A6ACA pendant chains favors the accessibility of the terminal carboxyl groups at the interface promoting nucleation [27,37]. We have previously shown that the mineral environment formed through biomineralization is osteoinductive and can promote stem cell differentiation in the absence of osteogenic medium [32,33,38–40]. This enables the use of partially-loaded constructs (top and middle layers loaded with cells) and chondrogenic inducing medium for preconditioning the constructs prior to their implantation and thereby circumvents the limitations associated with cocktail medium.

When implanted *in vivo*, the trilayer scaffolds loaded with cells in the top and middle layers and pre-conditioned for chondrogenesis resulted in osteochondral tissue formation. As designed, the cells loaded in the top and middle layer were confined within the respective layers and continued to undergo chondrogenic differentiation *in vivo*. The continued differentiation of hMSCs *in vivo* could be attributed to their *ex vivo* commitment and also the presence of chondrocytes in the middle layer. Chondrocytesecreted factors have been reported to promote chondrogenesis and prevent hypertrophic differentiation of stem cells [21,28,30,31,35]. Besides these biochemical cues, the layerspecific pore-architecture of the scaffold could have also played a role in the tissue formation and their organization. Hydrogels have been considered as an ideal scaffold for cartilage tissue engineering due to their large water content and ability to support spherical shape of the encapsulated cells [41,42]. The columnar-like alignment of chondrocytes is a key feature of deep and middle zones of articular cartilage [43]. The fact that the cells in the middle layer appeared to align vertically and the cells in the top layer align horizontally suggests a structurally-driven organization of the cells. The immunohistochemical staining of the *in vivo* engineered osteochondral tissue suggests that the cells in the top layer secreted lubricin. Lubricin, also known as superficial zone protein (SZP), is produced by chondrocytes in the superficial zone

and serves as an important boundary lubricant [44–46]. Interestingly, the presence of lubricin was observed only with the *in vivo* engineered tissue and not with the *in vitro* engineered tissue. The presence of lubricin in *in vivo* engineered tissue could be due to the shear force encountered by the implant subcutaneously, where the top layer of the implant facing the skin was subject to sliding motion with the movement of the animal. A number of studies have shown the importance of shear force in stimulating lubricin secretion by the chondrocytes [47–49].

The presence of cells in the bottom layer of the scaffold after their implantation suggests recruitment of endogenous cells by the mineralized layer. This is in accordance with our prior studies, which have shown that such macroporous biomineralized matrices can assist ectopic as well as orthotopic bone tissue formation through recruitment of endogenous cells from the host [26,33,34]. While the macroscopic pore structure could facilitate endogenous cell recruitment, their differentiation into osteogenic lineage and contribution to neo-bone tissue requires the mineral milieu of the scaffold [50]. We have shown that the mineral environment promotes osteogenic differentiation of cells, while inhibiting their differentiation towards adipogenesis, through phosphate-ATP-adenosine signaling axes [40,51]. The mineralized material-mediated adenosine signaling might have also contributed to the tissue formation. Adenosine signaling via the P1 receptor family of G protein-coupled receptors plays a key role in bone formation and homeostasis [52,53]. Recently, emerging studies have shown that adenosine signaling also plays a key role in regulating chondrocyte function and cartilage homeostasis [54,55]. Taken together, the single-unit scaffold may have provided a combination of chemical and structural cues that support osteochondral tissue formation. Although the outcome is encouraging from the subcutaneous model adopted in the current proof-ofconcept study, future works involving joint repair are needed to examine the efficacy of the trilayer scaffold in orthotopic tissue regeneration at load-bearing sites.

5. Conclusions

In summary, we developed a trilayer scaffold with depthvarying pore architecture and differential mineral environment to create osteochondral tissue. The scaffold included a biomineralized, interconnected macroporous layer recapitulating bone mineral microenvironment and a bilayer structure emulating certain architectural features such as stratification of native cartilage tissue. Combining the trilayer scaffold with stem cells and endogenous cells from the host, we demonstrate the formation of an engineered, anatomical analog of osteochondral tissue with lubricin positive cartilage surfaces *in vivo*. While the cartilage layer formation was achieved through the exogenous cells, the formation of bone layer relied upon the recruitment of endogenous cells and their differentiation into bone cells by the biomineralized layer.

Supplementary Material

Refer to Web version on PubMed Central for supplementary material.

Acknowledgements

Authors gratefully acknowledge the financial support by the National Institute of Arthritis and Musculoskeletal and Skin Diseases of the National Institutes of Health under Award Number R01 AR063184 and AR071552. The content is solely the responsibility of the authors and does not necessarily represent the official views of the National Institutes of Health. The hMSCs used in this study were provided by Texas A&M University (NIH, Grant P40RR017447).

References

[1]. Huey DJ, Hu JC, Athanasiou KA, Unlike bone, cartilage regeneration remains elusive, Science 338 (6109) (2012) 917–921. [PubMed: 23161992]

[2]. Baumbach K, Petersen J-P, Ueblacker P, Schröder J, Göpfert C, Stork A, Rueger JM, Amling M, Meenen NM, The fate of osteochondral grafts after autologous osteochondral transplantation: a one-year follow-up study in a minipig model, Arch. Orthop. Trauma Surg 128 (11) (2008) 1255–1263. [PubMed: 18064477]

[3]. Gomoll AH, Madry H, Knutsen G, van Dijk N, Seil R, Brittberg M, Kon E, The subchondral bone in articular cartilage repair: current problems in the surgical management, Knee Surg. Sports Traumatol. Arthrosc 18 (4) (2010) 434–447. [PubMed: 20130833]

[4]. Klein TJ, Malda J, Sah RL, Hutmacher DW, Tissue engineering of articular cartilage with biomimetic zones, Tiss. Eng. Part B: Rev 15 (2) (2009) 143–157.

[5]. O'Shea TM, Miao X, Bilayered scaffolds for osteochondral tissue engineering, Tiss. Eng. Part B: Rev 14 (4) (2008) 447–464.

[6]. Grayson WL, Chao P-HG, Marolt D, Kaplan DL, Vunjak-Novakovic G, Engineering custom-designed osteochondral tissue grafts, Trends Biotechnol 26 (4) (2008) 181–189. [PubMed: 18299159]

[7]. Seidi A, Ramalingam M, Elloumi-Hannachi I, Ostrovidov S, Khademhosseini A, Gradient biomaterials for soft-to-hard interface tissue engineering, Acta Biomater 7 (4) (2011) 1441–1451. [PubMed: 21232635]

[8]. Kon E, Delcogliano M, Filardo G, Fini M, Giavaresi G, Francioli S, Martin I, Pressato D, Arcangeli E, Quarto R, Orderly osteochondral regeneration in a sheep model using a novel nano-composite multilayered biomaterial, J. Orthop. Res 28 (1) (2010) 116–124. [PubMed: 19623663]

[9]. Martin I, Miot S, Barbero A, Jakob M, Wendt D, Osteochondral tissue engineering, J. Biomech 40 (4) (2007) 750–765. [PubMed: 16730354]

[10]. Harley BA, Lynn AK, Wissner-Gross Z, Bonfield W, Yannas IV, Gibson LJ, Design of a multiphase osteochondral scaffold III: fabrication of layered scaffolds with continuous interfaces, J. Biomed. Mater. Res 92A (3) (2010) 1078–1093.

[11]. Bhumiratana S, Eton RE, Oungoulian SR, Wan LQ, Ateshian GA, Vunjak-Novakovic G, Large, stratified, and mechanically functional human cartilage grown in vitro by mesenchymal condensation, Proc. Natl. Acad. Sci. USA 111 (19) (2014) 6940–6945. [PubMed: 24778247]

[12]. Chen J, Chen H, Li P, Diao H, Zhu S, Dong L, Wang R, Guo T, Zhao J, Zhang J, Simultaneous regeneration of articular cartilage and subchondral bone in vivo using MSCs induced by a spatially controlled gene delivery system in bilayered integrated scaffolds, Biomaterials 32 (21) (2011) 4793–4805. [PubMed: 21489619]

[13]. Sharma B, Elisseeff JH, Engineering structurally organized cartilage and bone tissues, Ann. Biomed. Eng 32 (1) (2004) 148–159. [PubMed: 14964730]

[14]. Nukavarapu SP, Dorcemus DL, Osteochondral tissue engineering: current strategies and challenges, Biotechnol. Adv 31 (5) (2013) 706–721. [PubMed: 23174560]

[15]. Filardo G, Madry H, Jelic M, Roffi A, Cucchiarini M, Kon E, Mesenchymal stem cells for the treatment of cartilage lesions: from preclinical findings to clinical application in orthopaedics, Knee Surg. Sports Traumatol. Arthrosc 21 (8) (2013) 1717–1729. [PubMed: 23306713]

[16]. Hwang NS, Zhang C, Hwang YS, Varghese S, Mesenchymal stem cell differentiation and roles in regenerative medicine, Wiley Interdiscip. Rev. Syst. Biol. Med 1 (1) (2009) 97–106. [PubMed: 20835984]

[17]. Discher DE, Mooney DJ, Zandstra PW, Growth factors, matrices, and forces combine and control stem cells, Science 324 (5935) (2009) 1673–1677. [PubMed: 19556500]

[18]. Lutolf MP, Gilbert PM, Blau HM, Designing materials to direct stem-cell fate, Nature 462 (7272) (2009) 433–441. [PubMed: 19940913]

[19]. Marklein RA, Burdick JA, Controlling stem cell fate with material design, Adv. Mater 22 (2) (2010) 175–189. [PubMed: 20217683]

[20]. Tuli R, Nandi S, Li W-J, Tuli S, Huang X, Manner PA, Laquerriere P, Nöth U, Hall DJ, Tuan RS, Human mesenchymal progenitor cell-based tissue engineering of a single-unit osteochondral construct, Tissue Eng 10 (7–8) (2004) 1169–1179. [PubMed: 15363173]

[21]. Hwang NS, Varghese S, Puleo C, Zhang Z, Elisseeff J, Morphogenetic signals from chondrocytes promote chondrogenic and osteogenic differentiation of mesenchymal stem cells, J. Cell. Physiol 212 (2) (2007) 281–284. [PubMed: 17520697]

[22]. Wang X, Wenk E, Zhang X, Meinel L, Vunjak-Novakovic G, Kaplan DL, Growth factor gradients via microsphere delivery in biopolymer scaffolds for osteochondral tissue engineering, J. Control. Release 134 (2) (2009) 81–90. [PubMed: 19071168]

[23]. Ayala R, Zhang C, Yang D, Hwang Y, Aung A, Shroff SS, Arce FT, Lal R, Arya G, Varghese S, Engineering the cell–material interface for controlling stem cell adhesion, migration, and differentiation, Biomaterials 32 (15) (2011) 3700–3711. [PubMed: 21396708]

[24]. Grayson WL, Bhumiratana S, Chao PG, Hung CT, Vunjak-Novakovic G, Spatial regulation of human mesenchymal stem cell differentiation in engineered osteochondral constructs: effects of pre-differentiation, soluble factors and medium perfusion, Osteoarthr. Cartilage 18 (5) (2010) 714–723.

[25]. Zhang C, Aung A, Liao L, Varghese S, A novel single precursor-based biodegradable hydrogel with enhanced mechanical properties, Soft Matter 5 (20) (2009) 3831–3834.

[26]. Varghese, Effect of scaffold microarchitecture on osteogenic differentiation of human mesenchymal stem cells, Eur. Cells Mater 25 (2013) 114–129.

[27]. Phadke A, Zhang C, Hwang Y, Vecchio K, Varghese S, Templated mineralization of synthetic hydrogels for bone-like composite materials: role of matrix hydrophobicity, Biomacromolecules 11 (8) (2010) 2060–2068. [PubMed: 20690714]

[28]. Varghese S, Hwang NS, Ferran A, Hillel A, Theprungsirikul P, Canver AC, Zhang Z, Gearhart J, Elisseeff J, Engineering musculoskeletal tissues with human embryonic germ cell derivatives, Stem Cells 28 (4) (2010) 765–774. [PubMed: 20178108]

[29]. Zhang C, Sangaj N, Hwang Y, Phadke A, Chang C-W, Varghese S, Oligo (trimethylene carbonate)–poly (ethylene glycol)–oligo (trimethylene carbonate) triblock-based hydrogels for cartilage tissue engineering, Acta Biomater 7 (9) (2011) 3362–3369. [PubMed: 21664305]

[30]. Aung A, Gupta G, Majid G, Varghese S, Osteoarthritic chondrocyte–secreted morphogens induce chondrogenic differentiation of human mesenchymal stem cells, Arthritis Rheum 63 (1) (2011) 148–158. [PubMed: 20954186]

[31]. Bian L, Zhai DY, Mauck RL, Burdick JA, Coculture of human mesenchymal stem cells and articular chondrocytes reduces hypertrophy and enhances functional properties of engineered cartilage, Tissue Eng. Part A 17 (7–8) (2011) 1137–1145. [PubMed: 21142648]

[32]. Kang H, Wen C, Hwang Y, Shih Y-RV, Kar M, Seo SW, Varghese S, Biomineralized matrix-assisted osteogenic differentiation of human embryonic stem cells, J. Mater. Chem. B 2 (34) (2014) 5676–5688. [PubMed: 25114796]

[33]. Shih Y-R, Phadke A, Yamaguchi T, Kang H, Inoue N, Masuda K, Varghese S, Synthetic bone mimetic matrix-mediated in situ bone tissue formation through host cell recruitment, Acta Biomater 19 (2015) 1–9. [PubMed: 25805106]

[34]. Shih Y-R, Kang H, Rao V, Chiu Y-J, Kwon SK, Varghese S, vivo engineering of bone tissues with hematopoietic functions and mixed chimerism, Proc. Natl. Acad. Sci 114 (21) (2017) 5419–5424. [PubMed: 28484009]

[35]. Levorson EJ, Santoro M, Kurtis Kasper F, Mikos AG, Direct and indirect co-culture of chondrocytes and mesenchymal stem cells for the generation of polymer/extracellular matrix hybrid constructs, Acta Biomater 10 (5) (2014) 1824–1835. [PubMed: 24365703]

[36]. Varghese S, Hwang NS, Canver AC, Theprungsirikul P, Lin DW, Elisseeff J, Chondroitin sulfate based niches for chondrogenic differentiation of mesenchymal stem cells, Matrix Biol 27 (1) (2008) 12–21. [PubMed: 17689060]

[37]. Phadke A, Zhang C, Arman B, Hsu C-C, Mashelkar RA, Lele AK, Tauber MJ, Arya G, Varghese S, Rapid self-healing hydrogels, Proc. Natl. Acad. Sci 109 (12) (2012) 4383–4388. [PubMed: 22392977]

[38]. Phadke A, Shih Y-RV, Varghese S, Mineralized synthetic matrices as an instructive microenvironment for osteogenic differentiation of human mesenchymal stem cells, Macromol. Biosci 12 (8) (2012) 1022–1032. [PubMed: 22760917]

[39]. Wen C, Kang H, Shih YR, Hwang Y, Varghese S, In vivo comparison of biomineralized scaffold-directed osteogenic differentiation of human embryonic and mesenchymal stem cells, Drug Deliv. Transl. Res 6 (2) (2016) 121–131. [PubMed: 26105532]

[40]. Kang H, Shih Y-RV, Varghese S, Biomineralized matrices dominate soluble cues to direct osteogenic differentiation of human mesenchymal stem cells through adenosine signaling, Biomacromolecules 16 (3) (2015) 1050–1061. [PubMed: 25686297]

[41]. Bryant SJ, Anseth KS, Hydrogel properties influence ECM production by chondrocytes photoencapsulated in poly(ethylene glycol) hydrogels, J. Biomed. Mater. Res 59 (1) (2002) 63–72. [PubMed: 11745538]

[42]. Varghese S, Theprungsirikul P, Ferran A, Hwang N, Canver A, Elisseeff J, Chondrogenic differentiation of human embryonic germ cell derived cells in hydrogels, Conf. Proc. IEEE Eng. Med. Biol. Soc 1 (2006) 2643–2646. [PubMed: 17946525]

[43]. Sophia Fox AJ, Bedi A, Rodeo SA, The basic science of articular cartilage: structure, composition, and function, Sports, Health 1 (6) (2009) 461–468. [PubMed: 23015907]

[44]. Schumacher BL, Block J, Schmid T, Aydelotte M, Kuettner K, A novel proteoglycan synthesized and secreted by chondrocytes of the superficial zone of articular cartilage, Arch. Biochem. Biophys 311 (1) (1994) 144–152. [PubMed: 8185311]

[45]. Zappone B, Greene GW, Oroudjev E, Jay GD, Israelachvili JN, Molecular aspects of boundary lubrication by human lubricin: effect of disulfide bonds and enzymatic digestion, Langmuir 24 (4) (2008) 1495–1508. [PubMed: 18067335]

[46]. Bao J-P, Chen W-P, Wu L-D, Lubricin: a novel potential biotherapeutic approaches for the treatment of osteoarthritis, Mol. Biol. Rep 38 (5) (2011) 2879–2885. [PubMed: 20099082]

[47]. Nugent GE, Aneloski NM, Schmidt TA, Schumacher BL, Voegtline MS, Sah RL, Dynamic shear stimulation of bovine cartilage biosynthesis of proteoglycan 4, Arthrit. Rheum 54 (6) (2006) 1888–1896.

[48]. Nugent-Derfus GE, Takara T, O'Neill JK, Cahill SB, Gortz S, Pong T, Inoue H, Aneloski NM, Wang WW, Vega KI, Klein TJ, Hsieh-Bonassera ND, Bae WC, Burke JD, Bugbee WD, Sah RL, Continuous passive motion applied to whole joints stimulates chondrocyte biosynthesis of PRG4, Osteoarthr. Cartilage 15 (5) (2007) 566–574.

[49]. Kamiya T, Tanimoto K, Tanne Y, Lin YY, Kunimatsu R, Yoshioka M, Tanaka N, Tanaka E, Tanne K, Effects of mechanical stimuli on the synthesis of superficial zone protein in chondrocytes, J. Biomed. Mater. Res. A 92 (2) (2010) 801–805. [PubMed: 19280634]

[50]. Gonzalez Diaz E, Shih Y, Nakasaki M, Liu M, Varghese S, Mineralized biomaterials mediated repair of bone defects through endogenous cells, Tissue Eng (ja) (2018).

[51]. Shih Y-RV, Hwang Y, Phadke A, Kang H, Hwang NS, Caro EJ, Nguyen S, Siu M, Theodorakis EA, Gianneschi NC, Vecchio KS, Chien S, Lee OK, Varghese S, Calcium phosphate-bearing matrices induce osteogenic differentiation of stem cells through adenosine signaling, Proc. Natl. Acad. Sci (111(3), 2014,) 990–995. [PubMed: 24395775]

[52]. Ham J, Evans BA, An emerging role for adenosine and its receptors in bone homeostasis, Front. Endocrinol. (Lausanne) 3 (2012) 113. [PubMed: 23024635]

[53]. Mediero A, Cronstein BN, Adenosine and bone metabolism, Trends Endocrinol. Metab 24 (6) (2013) 290–300. [PubMed: 23499155]

[54]. Tesch AM, MacDonald MH, Kollias-Baker C, Benton HP, Endogenously produced adenosine regulates articular cartilage matrix homeostasis: enzymatic depletion of adenosine stimulates matrix degradation, Osteoarthr. Cartilage 12 (5) (2004) 349–359.

[55]. Corciulo C, Lendhey M, Wilder T, Schoen H, Cornelissen AS, Chang G, Kennedy OD, Cronstein BN, Endogenous adenosine maintains cartilage homeostasis and exogenous adenosine inhibits osteoarthritis progression, Nat. Commun 8 (2017) 15019. [PubMed: 28492224]

Statement of Significance

In this work, we describe the use of a single-unit trilayer scaffold with depth-varying pore architecture and mineral environment to engineer osteochondral tissues *in vivo*. The trilayer scaffold was designed to support continued differentiation of the donor cells to form cartilage tissue while supporting bone formation through recruitment of endogenous cells. When implanted *in vivo*, these trilayer scaffolds partially loaded with cells resulted in the formation of osteochondral tissue with a lubricin-rich cartilage surface. Approaches such as the one presented here that integrates *ex vivo* tissue engineering along with endogenous cell-mediated tissue engineering can have a significant impact in tissue engineering composite tissues with diverse cell populations and functionality.

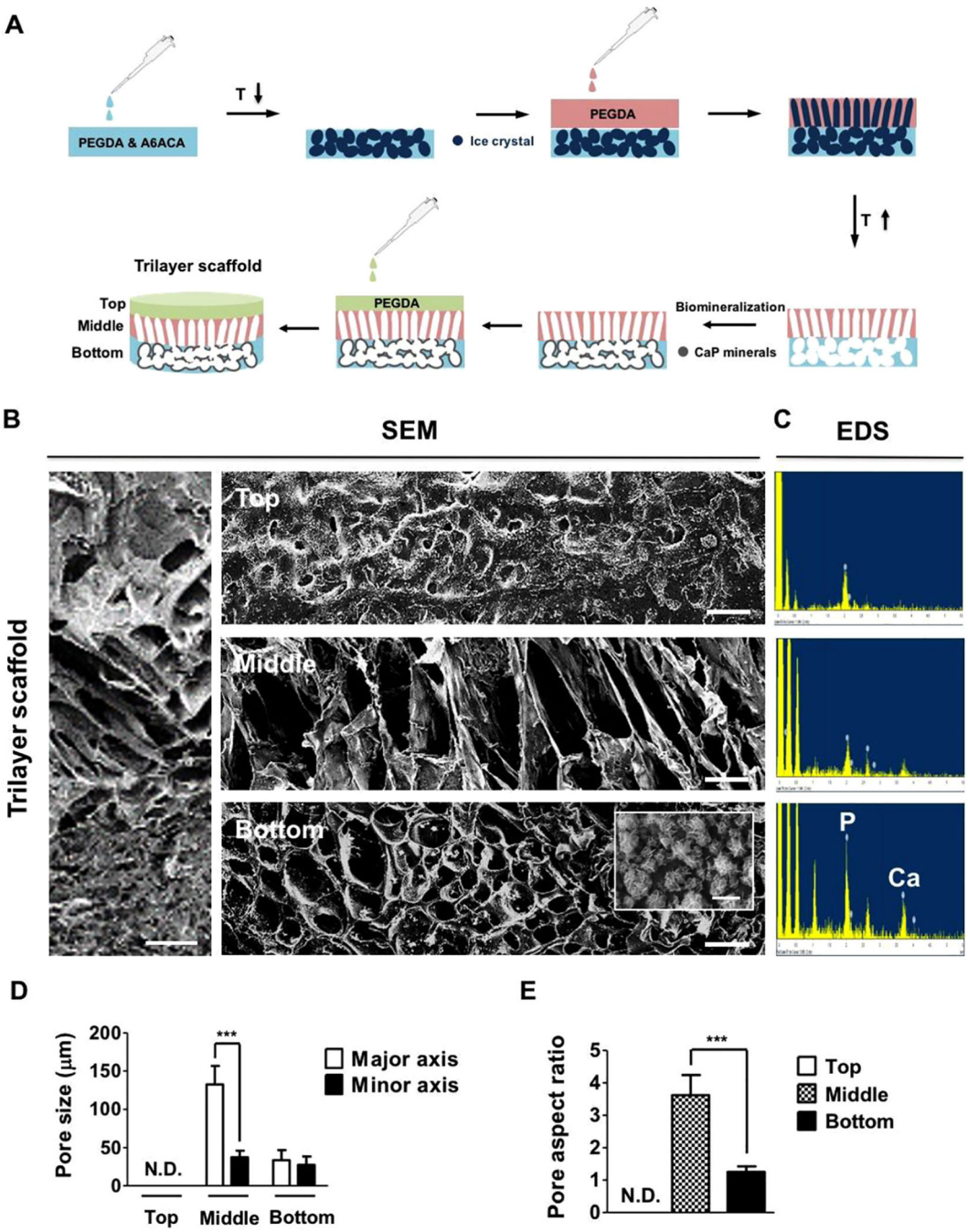

Fig. 1.

Trilayer scaffold exhibits layer-dependent varying pore microstructure and CaP biominerals. (A) Schematic for stepwise synthesis of the trilayer scaffold. (B) Scanning electron microscopy (SEM) image for cross-section of the trilayer scaffold. Scale bar represents 200 μm. High magnification SEM images of top, middle, and bottom layers of the trilayer scaffold are also shown. Scale bars indicate 50 μm. Inset shows a close-up SEM image of CaP biominerals in the bottom layer of the trilayer scaffold. Scale bar represents 2 μm. (C) Energy dispersive spectra (EDS) of top, middle, and bottom layers of the trilayer scaffold.

(D) Pore size in major and minor axes as well as (E) pore aspect ratio calculated from SEM images of top, middle, and bottom layers of the trilayer scaffold. N.D. indicates non-detectable pores from the top layer of the trilayer scaffold. The data are presented as mean ± standard deviations (n = 30). Two-tailed Student's *t*-test was used to compare two groups. Asterisks indicate statistical significances according to *p*-values ($^{***}p < 0.001$).

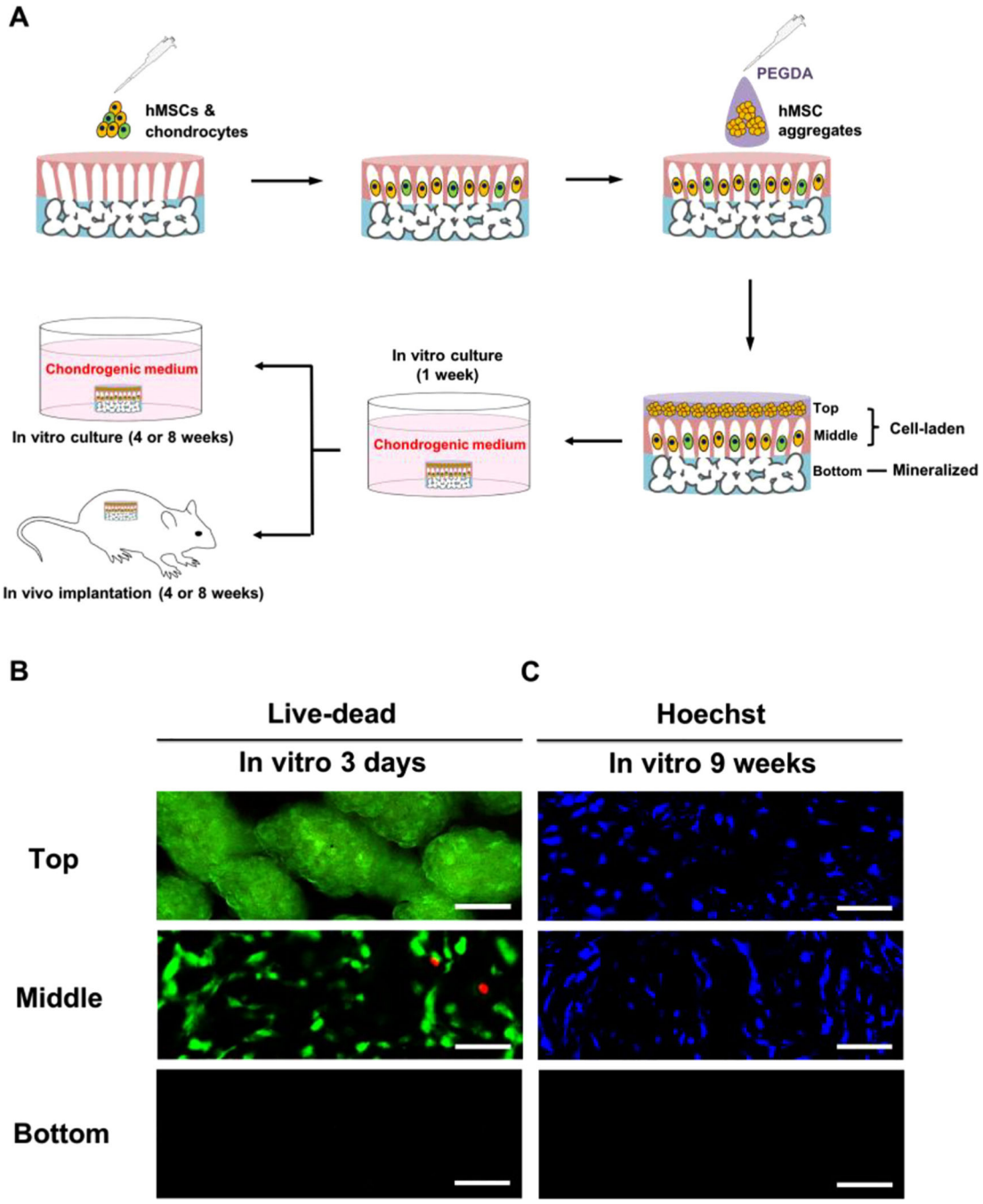

Fig. 2.

The cell-laden trilayer scaffold conduces to stratified cellular alignment after *in vitro* culture. (A) Schematic for an experimental protocol used to examine tissue-forming ability of the cell-laden trilayer scaffold both *in vitro* and *in vivo*. (B) Fluorescent live-dead staining for top, middle, and bottom layers of the cell-laden trilayer scaffold after 3 days of *in vitro* culture. (C) Fluorescent nucleus (Hoechst) staining for top, middle, and bottom layers of the cell-laden trilayer scaffold following 9 weeks of *in vitro* culture. Scale bars represent 50 μm.

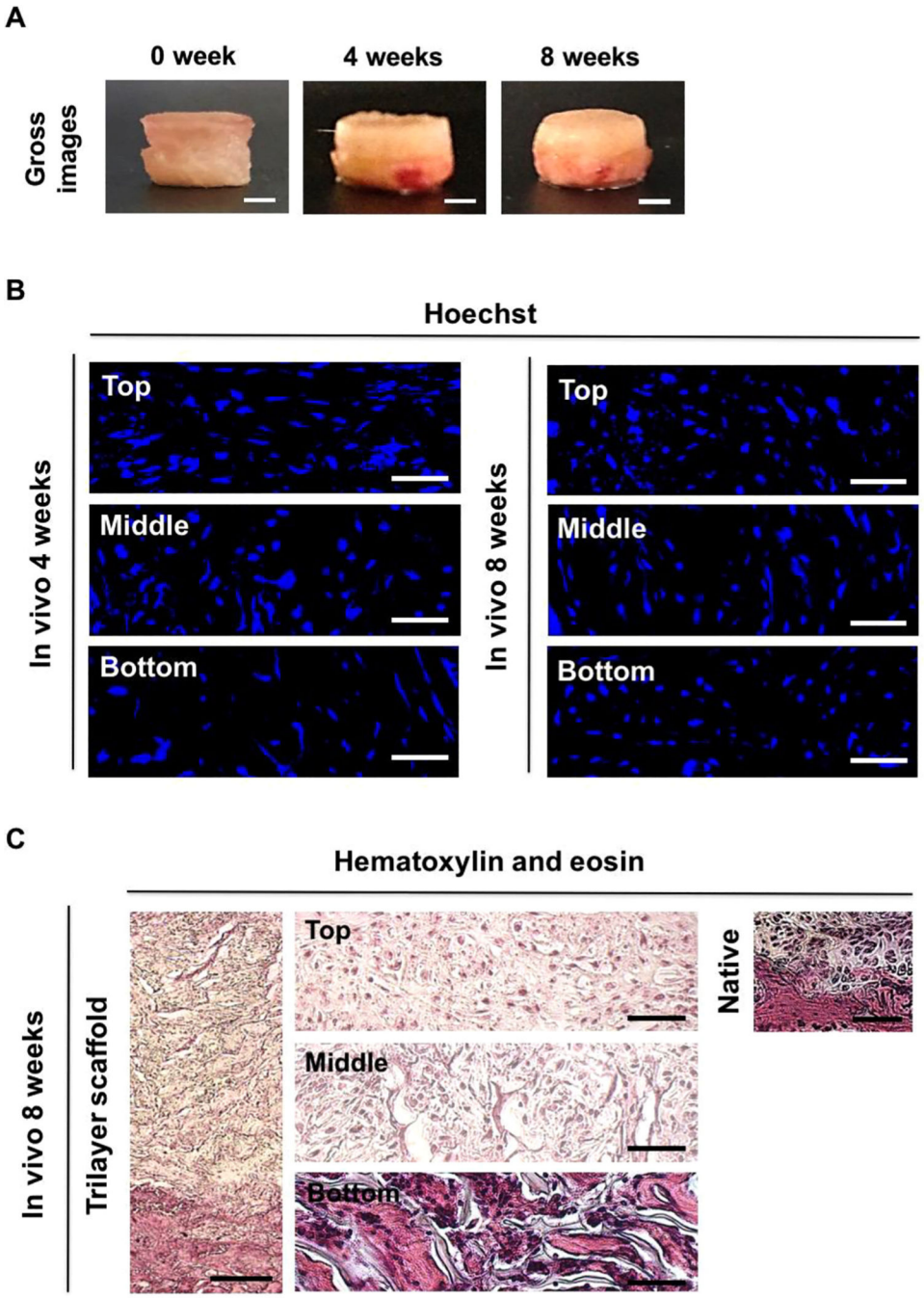

Fig. 3.

The cell-laden trilayer scaffold facilitates the formation of integrated, distinct cartilageand bone-like tissues *in vivo*. (A) Gross images of the cell-laden trilayer scaffold after 0, 4, and 8 weeks of *in vivo* implantation. Scale bars indicate 2 mm. (B) Fluorescent nucleus (Hoechst) staining for top, middle, and bottom layers of the cell-laden trilayer scaffold after 4 and 8 weeks of *in vivo* implantation. Scale bars represent 50 μm. (C) H&E staining of the cell-laden trilayer scaffold following 8 weeks of implantation. Scale bar indicates 200 μm. High

magnification images for top, middle, and bottom layers of the trilayer scaffold as well as native osteochondral tissue are also provided. Scale bars represent 50 μm.

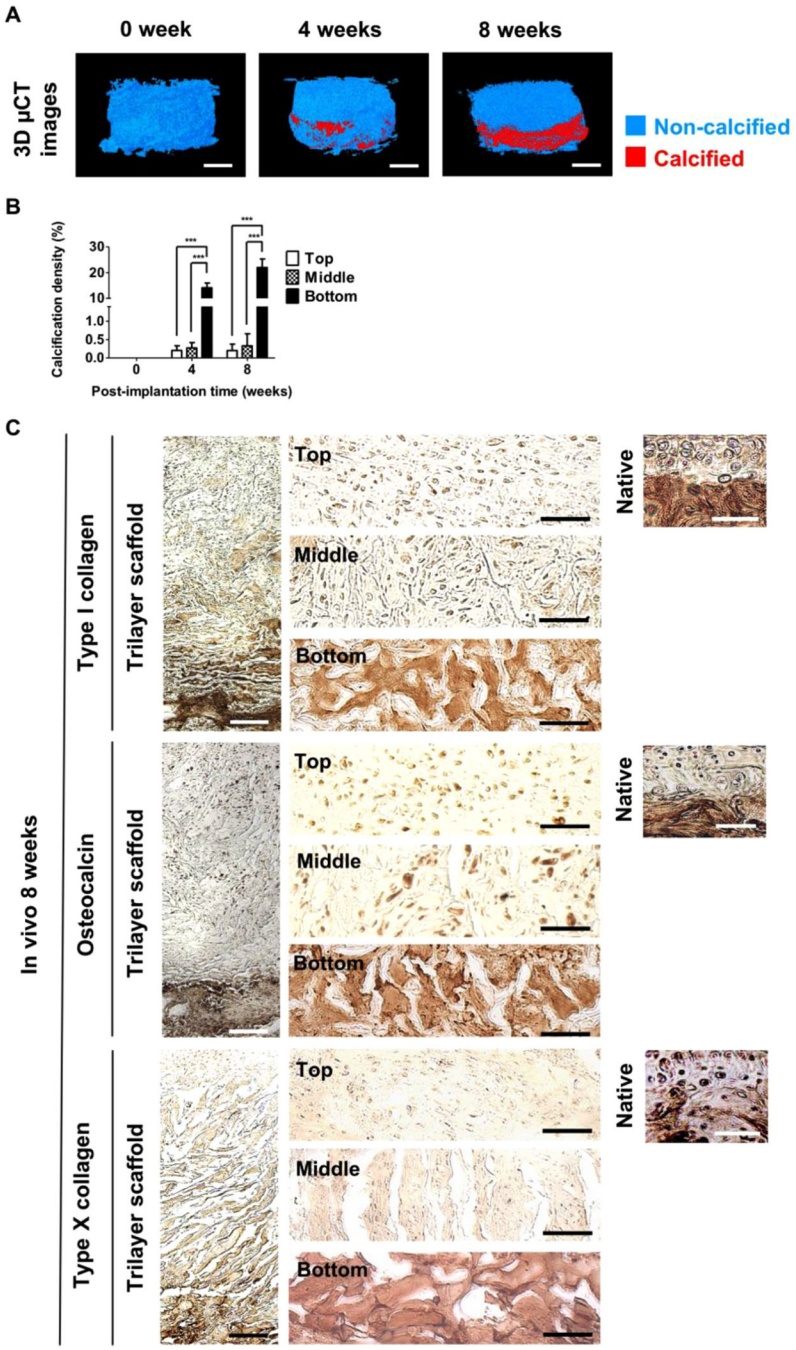

Fig. 4.

The acellular biomineralized bottom layer induces *de novo* formation of spongy bone *in vivo*. (A) 3D μCT models of the cell-laden trilayer scaffold after 0, 4, and 8 weeks of *in vivo* implantation. Calcified and non-calcified tissues are shown in red and blue, respectively. Scale bars indicate 2 mm. (B) Calcification density determined from 3D μCT models of top, middle, and bottom layers of the cell-laden trilayer scaffold as a function of post-implantation time. (C) Immunohistochemical staining for type I collagen, osteocalcin and type X collagen of the cell-laden trilayer scaffold following 8 weeks of implantation. Scale

bars indicate 200 μm. High magnification images for top, middle, and bottom layers of the trilayer scaffold as well as native osteochondral tissue are also provided. Scale bars represent 50 μm. Data are shown as mean ± standard errors (n = 6). Comparisons of multiple groups in the same time point were made by one-way ANOVA with Tukey-Kramer post-hoc test. Asterisks indicate statistical significances according to *p*-values ($^{***}p < 0.001$). (For interpretation of the references to color in this figure legend, the reader is referred to the web version of this article.)

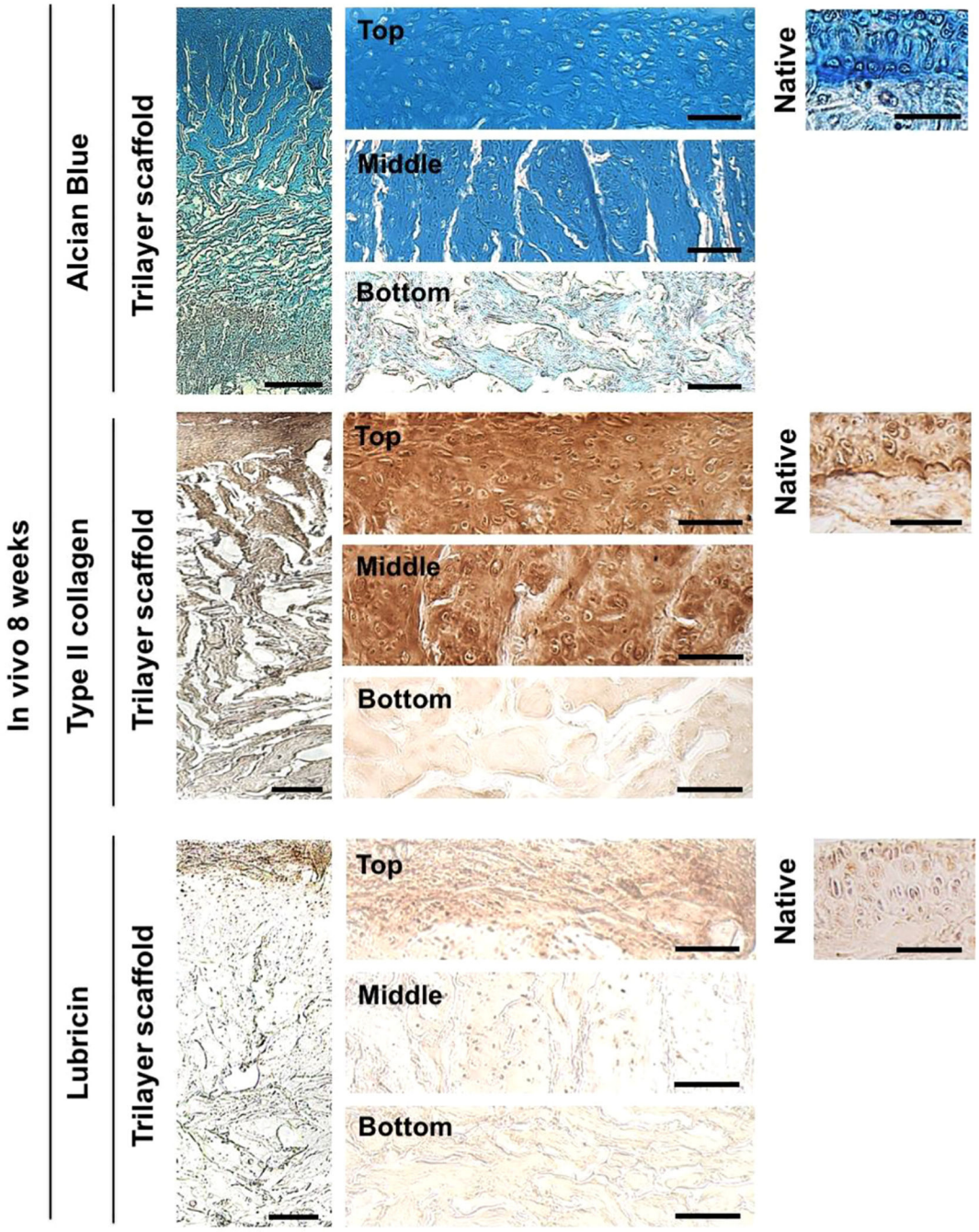

Fig. 5.

The cell-laden top and middle layers support *in vivo* formation of stratified cartilage with lubricin-rich surface. Alcian Blue staining and immunohistochemical staining for type II collagen and lubricin of the cell-laden trilayer scaffold at 8 weeks post-implantation. Scale bars represent 200 μm. High magnification images for top, middle, and bottom layers of the trilayer scaffold as well as native osteochondral tissue are also shown. Scale bars indicate 50 μm. (For interpretation of the references to color in this figure legend, the reader is referred to the web version of this article.)

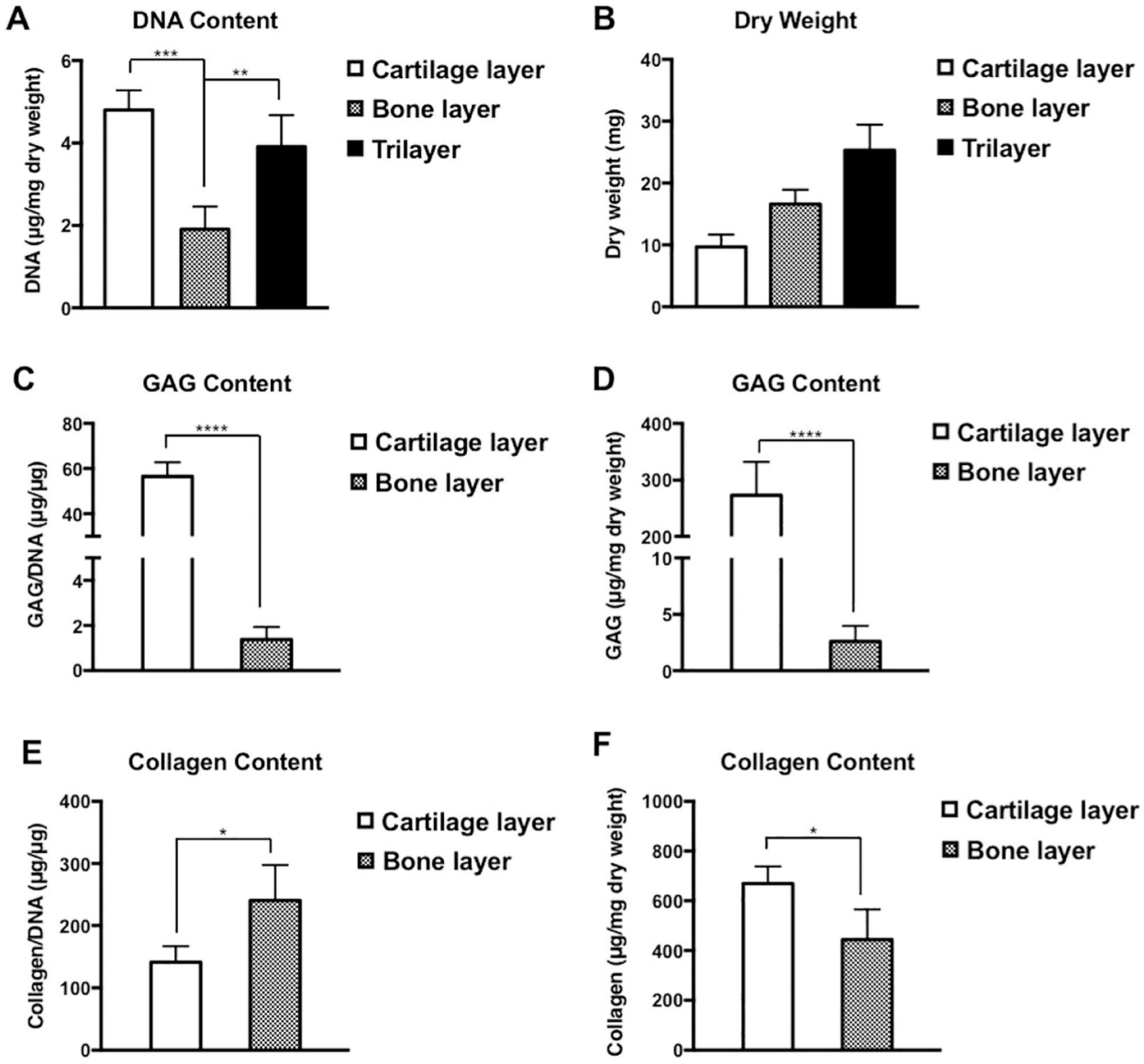

Fig. 6.

Biochemical analyses of the trilayer scaffold. The intact scaffold (Trilayer), its cell-laden top and middle layers (Cartilage layer), and the mineralized bottom layer (Bone layer) were prepared for quantifying the deposition of GAG and collagen after 8 weeks of subcutaneous implantation. (A) DNA content in the scaffolds. (B) Dry weight of the scaffolds. (C, D) GAG content, normalized to the DNA content and dry weight of the corresponding scaffold, respectively. (E, F) Collagen content, normalized to the DNA content and dry weight of the corresponding scaffold, respectively. Error bars show the mean ± SD (n = 8). Statistical significance was performed using one-way ANOVA with post hoc Tukey-Kramer test, *P < 0.1, **P < 0.01, ****P < 0.0001.